Structural Chemistry (2024) 35:553–567
https://doi.org/10.1007/s11224-023-02200-5

RESEARCH

Characterization and properties of a new insensitive explosive co-crystal composed of trinitrotoluene and pyrene

Nilgün Şen[1,2] · Nazife Aslan[3] · Bayram Yüksel[4] · Irem Teciman[1]

Received: 8 May 2023 / Accepted: 19 June 2023 / Published online: 29 July 2023
© The Author(s) 2023

Abstract

A new energetic co-crystal of trinitrotoluene (TNT) and pyrene (PYRN) with a 1:1 molar ratio was prepared by a slow solvent evaporation technique. Co-crystal physicochemical properties have also been examined using optical microscopy, powder X-ray diffraction, single crystal X-ray diffraction, and differential scanning calorimetry. The results of single-crystal X-ray diffraction and non-covalent interaction calculations showed that non-covalent interactions (donor–acceptor π-π interaction) govern the structures of the TNT:PYRN co-crystal. The experimental and theoretical outcomes supported each other in the study. Thermal stability, impact sensitivity, and detonation performance of the co-crystal were investigated. DSC measurement indicates that the co-crystal has a melting point of 167 °C and a decomposition temperature of 293 °C, indicating outstanding thermal stability. The co-crystal was found to be less impact-sensitive than TNT using the BAM fall hammer instrument. Furthermore, the calculated detonation velocity and detonation pressure of the co-crystal are 5.29 km·s^{-1} and 8.48 G Pa, respectively. As an outcome, the TNT:PYRN co-crystal may be a promising intermediate energy explosive with low sensitivity and, as such, may be a desirable explosive alternative in the future instead of TNT for low-vulnerability formulations.

Keywords Non-covalent interactions · Trinitrotoluene · Pyrene · Impact sensitivity · Energetic co-crystals

Introduction

Energetic materials (explosives, propellants, and pyrotechnics) (EMs), which store a great amount of chemical energy in their molecular structures, quickly release the chemical energy and form a mass of gases when exposed to high temperature and high pressure. EMs are widely used in military and civilian applications because they can cause propulsion or damage through explosion or combustion [1–4]. Despite the potentially massive risks, EMs are incomparable to other types of materials because to their special qualities of rapid release of energy in the form of gas and heat. In spite of a long history of almost 1200 years, they have progressed relatively slowly in terms of power as a fundamental property. For example, the detonation velocity has increased only 30% over the last century from TNT to HMX and CL-20, which are considered to be representations of the first, second, and third generations of EMs, respectively. Despite the development of various new EMs, their comprehensive properties can hardly outperform [5–9]. The reason for the slow evolution can be attributed to the composition limitation of CHON elements [10], the energy – safety contradiction [11–13], the low-efficiency design and synthesis, and the multiple and strict requirements for use [4]. However, this does not indicate that we should stop our efforts to develop new EMs. Instead of pursuing high energy alone, we can aim to make full use of existing molecules or create new compounds with outstanding comprehensive features. Many searches are focused on generating energy-safety balanced EMs [7–9]. This might be linked to materials with low sensitivity and high energy (LSHEM) [13]. In terms of EMs, they generally have the property that the more the energy,

✉ Nilgün Şen
nilgunsen2001@gmail.com; nilgun.sen@cranfield.ac.uk

1 Turkish National Police Academy, Institute of Forensic Sciences, Ankara, Turkey

2 Centre for Defence Chemistry, Cranfield University, Defence Academy of the United Kingdom, SN6 8LA Shrivenham, UK

3 Department of Chemistry, Polatlı Science and Arts Faculty, Ankara Hacı Bayram Veli University, Ankara, Turkey

4 Department of Property Protection and Security, Giresun University, Giresun, Turkey

the greater the impact sensitivity, as the well-known energy safety paradox suggests [11–13]. Only FOX-7, LLM-105, and NTO can now satisfy the LSHEM criteria, signalling a significant hurdle in producing an LSHEM via ordinary chemical synthesis.

In recent years, energetic co-crystallization has emerged as a viable alternative approach to novel Ems [14–18]. As a result, this technique is intended to alleviate the energy safety paradox and manufacture more LSHEMs [12]. In fact, the strategy is related to crystal engineering. Crystal engineering means understanding the intermolecular interactions and their effects on packing structures and properties and then applying that knowledge to produce new crystal materials with the desired attributes [19, 20] Crystal engineering has demonstrated its great power in developing new materials, as it has been widely applied in many fields, including material mechanics [21], polymorphic control [22], drug delivery [23, 24], coordination polymer construction [25], luminescence tuning [26], metalorganic framework construction [27, 28], and the construction of hydrogen-bonded or halogen-bonded systems [29–32]. The same is projected of EMs. Indeed, a considerable lot of success has been accomplished in designing novel low-sensitivity or desensitized Ems [12] based on an understanding of the effect sensitivity molecular stacking mode connection [33–36]. The physical and energetic characteristics of a few different co-crystal examples were compiled and contrasted with their constituents in order to clearly show the advantages of energetic co-crystals over their constituents (Table 1) [15, 16, 37–43]. The formation of these materials depended mainly on donor–acceptor π … π interactions between the electron-poor ring (energetic) and the electron-rich rings (energetic or non-energetic materials). It should be emphasized in light of these results that energetic co-crystals are best suited for creating powerful and safe explosives.

TNT, or 2,4,6-trinitrotoluene, was developed in 1863 and is still used as an explosive today [44]. It has poor performance and a detrimental environmental impact, yet it is nevertheless employed due to its low production costs and ability to be melt-cast [45]. At the same time, costly and time-consuming upgrading and purification activities are required. As a result, new, environmentally safe, non-toxic, and highly EMs must be developed, require careful handling and storage [46].

This paper presents a novel way to change the characteristics of existing EMs through co-crystallization. The structure and energetic properties of a novel co-crystal of the benchmark energetic substance TNT are revealed. The donor–acceptor interaction is a dependable supramolecular synthon for the creation of co-crystals with this aromatic energetic material. A detailed study of the co-crystal created reveals changes in critical parameters such as density, free space (voids) packing coefficient, melting point and decomposition temperature, impact sensitivity, detonation velocity, and pressure. The structure and energetic behaviour of the novel solid form TNT:PYRN were studied using a variety of experimental and computational methods, demonstrating that TNT:PYRN have enhanced thermal and mechanical stability but explosive performance has diminished to

Table 1 Physical and energetic properties of selected co-crystals compared with those of their components

Entry	T_m [a] (°C)	T_d [b] (°C)	ρ [c] (g·cm^{-3})	D [d] (km·s^{-1})	P [e] (GPa)	IS [f] (J)	Ref.
TNT	80	283	1.65	6.88	19.5	15	[38]
TNT:VANT	102	268.3	1.47	5.58	9.55	79.4	[39]
TNT:ATL	103	194	1.52	7.08	18.5	79.4	[40]
TNT:PYRN	167	292	1.49	5.29	8.48	70.8	This work
Ɛ-CL-20	145	227	2.03	9.40	44.6	4.0	[15, 37]
TNT:CL-20	136	205	1.84	-	-	55	[15]
HMX	-	280	1.91	9.32	39.5	55	[16, 37]
CL-20/HMX	-	235	1.51	9.48	-	55	[16]
BTF	198	289	1.90	8.42	34.3	-	[41]
CL-20/BTF	-	235	1.91	8.96	39.1	-	[41]
TZTN	144	197	1.57	7.27	21.6	6	[42]
NTO/TZTN	157	178	1.66	7.45	23.5	11	[42]
PIC	121	> 300	1.81	7.83	27.2	22.4	[43]
PIC:VANT	121.9	231.6	1.51	5.63	1.09	31.6	[39]

[a]Melting point (onset)

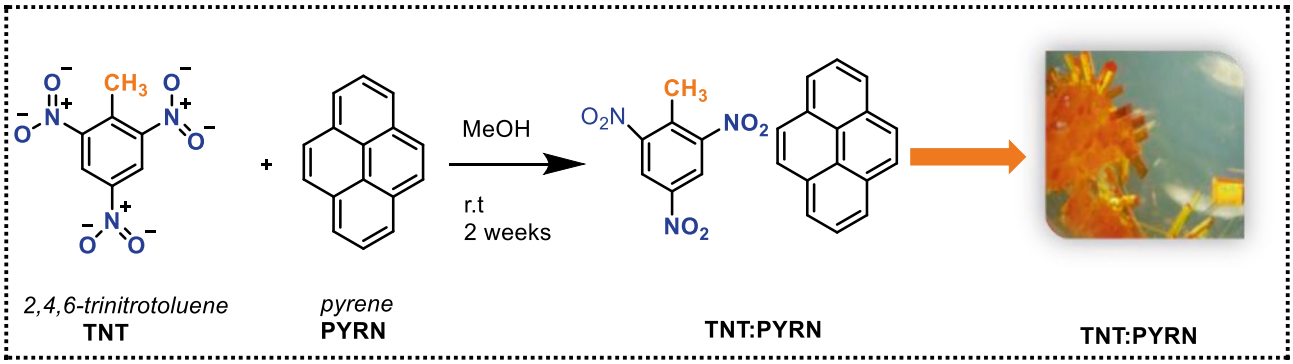
[b]Decomposition temperature (onset)

[c]Density

[d]Detonation velocity

[e]Detonation pressure

[f]Impact sensitivity



Scheme 1 Synthetic routes and co-crystal formation of TNT:PYRN host–guest type compound

some amount. Although non-energetic components generally dilute the energy content, they can considerably increase the number of energetic co-crystals, creating a rich database for following studies in a data-driven or crystal engineering way.

Experimental

Caution! All of these EMs were manufactured on a milligram scale, and none exploded or detonated during this experiment. Wear protective clothing such as leather suits and earplugs, as well as safety shields, safety glasses, face shields, and leather gloves.

Materials and sample preparation

PYRN (98%) and 2,4-diaminotoluene (97%) were obtained from Sigma-Aldrich. TNT was synthesized from 2,4-dinitrotoluene, depending on the literature [47]. Slow evaporation of a methanolic solution (4 mL) of TNT (75 mg, 1 equiv., at 50 °C) and PYRN (67 mg, 1 equiv.) resulted in the formation of single crystals of the co-crystal (TNT:PYRN) (Scheme 1).

Characterisation techniques

Single-crystal X-ray diffraction of the co-crystal was performed on an Agilent Technologies Super Nova diffractometer equipped with an Oxford Cryo Systems cryoprobe. The crystal was kept at $T = 120.0$ K during data collection. Using Olex2 [48], the structure was solved with the SHELXT [49] structure solution program, using the Intrinsic Phasing solution method. The model was refined with version 2017/1 of SHELXL [50] using least squares minimisation. Mercury CSD (v.4.1) software was used to aid in the structural study of the co-crystal [51].

PXRD patterns were obtained using the D2 PHASER Advance instrument using Cu-Kα radiation ($\lambda = 1.54439$ Å) and an operating voltage and current 40 kV and 40 Ma, respectively. The data were collected over an angle range of $2\theta = 5–50$. This technique provided an initial screening of samples for formation of co-crystals.

Optical micrographs of all the crystals were taken using an SK2005A polarization microscope.

Differential scanning calorimetry (DSC) was performed on a NETZSCH STA 449 F1 Differential Scanning Calorimeter. Approximately 1.5 mg of salt sample was placed in an aluminum pan and the thermal behavior of the sample was studied under a nitrogen purge (30.0 mL/min) at a heating rate of 10 °C/min over a temperature range from 25 to 400 °C.

Energetic performance and sensitivity

The impact sensitivity was measured using a BAM fall hammer (BFH-12). Impact testing was conducted at the Cavendish Laboratory, Cambridge, on the TNT, PYRN, and TNT:PYRN. A sample of 40 mm^3 approximate volume was enclosed in anvil device consisting of two coaxial steel cylinders. A load of 10 kg was dropped on to the sample from heights ranging from 10 to 100 cm. The "one-in-six" test procedure was performed to obtain the limiting impact energy for the tested sample. The method conducted throughout is the 30-trial Bruceton method [52, 53]. All detonation parameters such as detonation velocity, pressure, and oxygen balance, presented in this work, were determined from calculations using the program EXPLO5 v6.03 [54].

Computational methods

Hirshfeld surface analysis

To visualize and quantify distinct chemical interactions, an analysis of the Hirshfeld surfaces and the accompanying

2D fingerprint plots [55] was performed using the Crystal Explorer 3.0 [56] software package. The Hirshfeld surfaces were mapped over d_{norm} and shape index properties. The d_{norm} is a symmetric function of distances to the surface from nuclei inside and outside the Hirshfeld surfaces (d_i and d_e, respectively), relative to their respective van der Waals (vdW) radii, which enables the identification of critical areas for intermolecular interactions. It enables the identification of critical areas for intermolecular interactions. The d_{norm} surfaces were mapped over a fixed color scale of −0.086 au (red) and −0.605 Å au (blue) The color scale of the three-dimensional d_{norm} of the material is between -0.086 Å (red) and -0.605 Å (blue). The shape-index feature is based on the surface's local curvature and is particularly effective for identifying planar π-stacking arrangements [55].

Calculation of heat of formation (HOF)

In this paper, all ab initio calculations were carried out using the program package Gaussian 09 (Revision-D.01) [57] and visualized by GaussView 5.0.9 [58]. In order to calculate the energy of formations and the detonation parameters of compounds, the enthalpies (H) were computed according to the atomization energy method (Eq. (1); Table 2) [59, 60] based on the complete basis set method (CBS-4 M), which is included in the Gaussian program. Structure optimization, the distribution electron density in bonds between atoms, electrostatic potential, and electronic density were performed by the DFT-B3LYP method with a 6-31G (d, p) basis set in a gas phase. Energy minimization of PYRN was calculated with the 6–31 + G (d, p) basis set using the account diffusive function. Single-crystal X-ray was used as the input for each calculation. The stabilization of optimized structures was controlled with the number of image frequencies (NIMAG) by frequency analysis. In Eq. (1), where $\Delta H_f^\circ(g, M)$ represents the enthalpy of formation of the investigated molecule (M) in gas phase, $H^\circ_{(molecule)}$ stands for the calculated enthalpy value of the molecule M with the CBS-4 M method (H^{298} in Table 2); $\Sigma H^\circ_{(atoms)}$ denotes the summary of calculated enthalpies for the individual atoms (H, C, N, O; see Table 2) and $\Sigma\Delta H^\circ_{f(atoms)}$ stands for experimental values of the enthalpy of formation (ΔH_f°) for the corresponding atoms H, C, N, and O to be 217.100, 716.682, 472.679, and 249.178 kJ·mol^{-1}, respectively [61].

Table 2 Computed (CBS-4 M) and experimental (NIST [61]) values to be used for the enthalpy of formation calculation

Entry	P.G.	NIMAG[b]	$-H^{298}$ (a.u.)[c]	$-\Delta H_f^\circ$(kJ·mol^{-1})[d]
TNT	C_1	0	883.954543	25.557620
TNT:PYRN	C_1	0	1498.757295	33.859383
H			0.500991	217.100
C			37.786156	716.682
N			54.522462	472.679
O			74.991202	249.178

[a]Point group

[b]Number of imaginary frequencies

[c]Enthalpy values obtained from the CBS-4 M calculations

[d]Enthalpy of formation (in gas phase)

$$\Delta H_f^\circ(g, M) = H^\circ_{(molecule)} - \Sigma H^\circ_{(atoms)} + \Sigma\Delta H^\circ_{f(atoms)} \quad (1)$$

Visualization of electrostatic potential (ESP) map

An ESP is a representation of the electrostatic potential at the molecular surface, displayed through a color scheme. ESP charts are useful tools for visualizing the charge distribution within a molecule. The collected data can provide critical information for analyzing the potential electroactive sub-fragments of the target molecules, which can be used to construct chemical reactivity patterns. The electrostatic potential maps are color-coded, where positive (electron-deficient) regions are depicted in blue, and negative (electron-rich) regions are depicted in red. The green regions are considered to have zero electrostatic potential, while yellow regions indicate intermediate electron density. To summarize, the potential values represented by different colors can be ranked in a descending order as red > orange > yellow > green > blue. For this purpose, the preliminary findings of the geometry optimization analysis were employed to generate the ESP maps of TNT, PYRN, and TNT:PYRN.

Non-covalent interactions (NCIs)

The NCI study was carried out utilizing a computational methodology known as the reduced density gradient (RDG) technique [62, 63]. NCI patterns were investigated utilizing the output data from geometry optimization experiments performed using Gaussian 09 at the B3LYP-D3/def2-TZVP level of theory. Multiwfn software (v.3.8) [64] was used to generate the essential density gradients. Using the VMD (Visual Molecular Dynamics) program (v.1.9.3), these gradients were then utilized to generate the demonstration graphs [65].

Results and discussion

Microscope images

The slow evaporation technique was used to allow methanol to evaporate gradually over a 2-week period, resulting in the formation of the target TNT:PYRN in dark orange block-shaped crystals (Fig. 1b) (yield, 87%). The crystal shapes, sizes, and colour differ from those of their co-former (TNT in Fig. 1a).

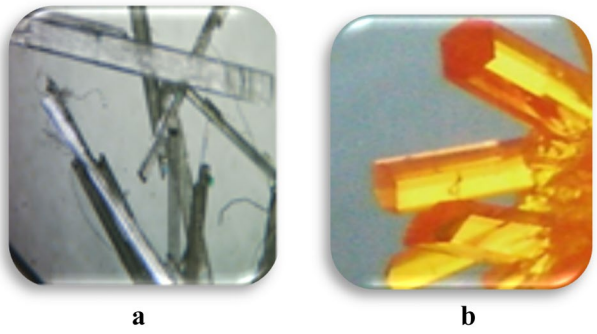


Fig. 1 Microscope images at × 50 magnification of **a** TNT and **b** TNT:PYRN

Determination of the TNT:PYRN crystal structure

Table 3 summarizes the crystallographic data obtained and the structural refinement results of TNT:PYRN. CCDC number **1818100** is obtained from the Cambridge Crystallographic Data Centre. The ORTEP drawing of TNT:PYRN and crystal structure are shown in Fig. 2a, b. The SCXRD analysis of TNT:PYRN is determined by selecting good-quality crystals of appropriate size (0.33 × 0.27 × 0.17). TNT:PYRN possesses the triclinic crystal system with the *P*-1 space group and a density of 1.503 g cm^{-3} (T = 120.0 K). TNT:PYRN co-crystal has an asymmetric unit consisting of one TNT and one PYRN.

The main non-covalent interaction occurs between the electron-rich and electron-poor aromatic rings, as in between the electron-poor π -system of TNT and the electron-rich π -system of PYRN (Fig. 10a–e). By measuring the excess formation enthalpy of the co-formers, the COSMOtherm [66] program was used to anticipate the likelihood of co-crystal formation while selecting electron-rich aromatic ring compounds. The Turbomole program was used to generate the calculations, which used the BP86 density functional with a TZVP34 basis set (BPTZVP-COSMO level of theory). The general rule is that a pair of materials with a ΔpKa (ΔpKa = pKa [protonated base] − pKa [acid]) more negative than − 1 will form a co-crystal (the pKa value of PYRN is > 15, while the pKa value of TNT is 16.99) [67]. When the pKa values of TNT and PYRN are evaluated, it becomes clear that new co-crystal is possible. The predominant non-covalent interaction occurs between electron-rich (PYRN) and electron-poor (TNT) aromatic rings. The slip distances and angles between TNT centroids and PYRN centroids were measured to be 3.65 (6) and 89.9 (1). The values are typical of aromatic face-to-face π-interactions (< 4.00 Å) [68] (Fig. 3).

Both mercury software measurements and non-covalent interaction (NCI) calculations show that the π… π interaction is prominent in the formation of TNT:PYRN co-crystal. When Table 4 is investigated, it is evident that several weak H bonds (C-H…O) are formed. These hydrogen bonds are extremely weak formed due to electrostatic interactions. Based on the NCl calculation results, van der Waals and the steric effects have a considerable effect on co-crystal formation. Molecules display a parallel face-to-face π-π interaction, with each side stacked alongside another molecule to form an edge-to-face arrangement.

Table 3 Crystallographic data and structure refinement parameters for TNT:PYRN

Empirical formula	$C_{23}H_{15}N_3O_6$
ρ_{calc}.(g·cm^{-3})	1.503
μ/mm^{-1}	0.932
Formula weight (g·mol^{-1})	429.37
Colour	Dark yellow
Shape	Block
Crystal size (mm^3)	0.33 × 0.27 × 0.17
T (K)	173 (2)
Crystal system	Triclinic
Space group	*P*-1
a (Å)	7.98360 (10)
b (Å)	14.7814 (3)
c (Å)	16.2678 (3)
α (°)	98.159 (2)
β (°)	90.748 (2)
γ (°)	92.709 (2)
Volume ($Å^3$)	1897.81 (6)
Z	4
Z'	2
Wavelength (Å)	1.54184
Radiation type	CuK_a
2Θ range for data collection/°	7.568 to 152.086
Q_{min}–Q_{max} (°)	3.784–76.043
Reflections collected	30,322
Independent reflections	7820 [R_{int} = 0.0709, R_{sigma} = 0.0465]
Reflections used	7243
R_{int}	0.0709
Data/restraints/parameters	7820/0/579
Largest peak	0.346
Deepest hole	−0.407
Goodness-of-fit on F^2	1.016
Final R indexes [$I \geq 2\sigma$ (I)]	R_1 = 0.0580, wR_2 = 0.1594
Final R indexes [all data]	R_1 = 0.0604, wR_2 = 0.1632
CCDC number	**1818100**

Powder X-ray diffraction analysis (PXRD)

PXRD of the TNT, PYRN, and TNT:PYRN is showed in Fig. 4. TNT:PYRN diffraction patterns are clearly distinct from TNT and PYRN diffraction patterns, confirming the formation of a new compound.

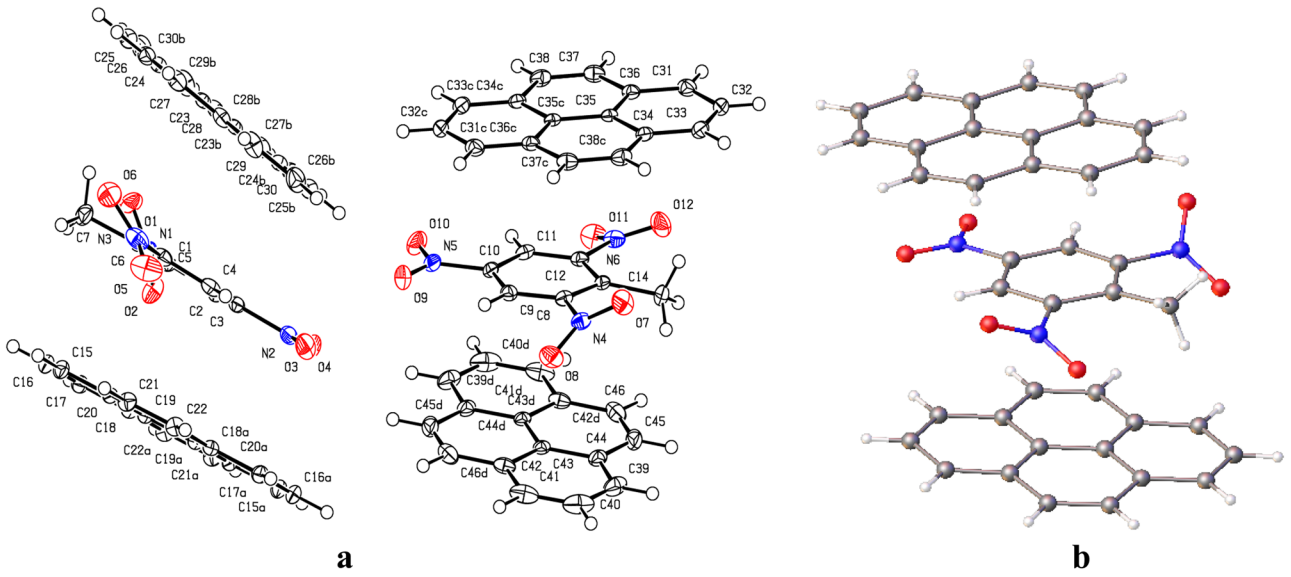


Fig. 2 ORTEP drawing of **a** TNT:PYRN and the asymmetric unit of the title compound, showing the atom-numbering scheme. Displacement ellipsoids are drawn at the 50% probability level. **b** Crystal structure of TNT:PYRN

Differential scanning calorimetry

The melting point and decomposition temperature of EMs are essential to determining their thermal stability. Figure 5a shows a DSC thermogram with two endotherms and one exotherm peak for TNT:PYRN. TNT is thought to have formed from an impurity at the first endotherm, 62.9 °C. The melting point of the TNT:PYRN co-crystal was measured to be 167 °C, which is greater than the melting point of TNT (83.5 °C) (Table 5). The melting point is determined by the lattice energy, or the total intermolecular interaction that occurs in a crystal cell [69]. The TNT:PYRN co-crystal was formed as a consequence of a π… π stacking interaction with weak hydrogen bonds, resulting in a considerably greater lattice energy than TNT. Intermolecular and non-covalent interactions may cause an increase in melting point. Furthermore, increasing the melting point can be beneficial for developing munitions that withstand deformation before explosion [14]. Co-crystallization can cause significant changes in another essential physical property of energetic materials. The mass loss for TNT:PYRN is 96.52% (Fig. 5).

Hirshfeld surface analysis

Hirshfeld surface (HS) studies were carried out in order to acquire a better knowledge of the packing motifs and the contributions of the key intermolecular interactions that influence the molecular architecture in crystalline compounds. HS mapped over the d_{norm} property in two orientations is shown in Fig. 6a. The surfaces are presented transparently to allow visualization of the molecules within the surfaces. Contacts with distances equal to the sum of the van der Waals radii are depicted in white, while contacts with distances less than and more than van der Waals radii are displayed in red and blue, respectively. The corresponding full two-dimensional fingerprint plots (FPs) of O…H, H…H, C…H, O…O, and C…C contacts are displayed in Fig. 7. In structure TNT:PYRN, the bright regions labeled represent H…O/O…H contacts associated to C-H…O hydrogen bonds, which are showed as a pair of symmetrical spikes at $d_e + d_i \approx 2.4$ Å in the corresponding FP plot. These comprise approximately 40% (O…H) of the entire TNT:PYRN HS. The 32% H…H interactions continue to be the most important contributors to the total Hirshfeld surfaces and can be seen as the "ridge" of the 2-D fingerprint plots. The pattern of red and blue triangles on the same region of the shape index surface in Fig. 8b is also characteristic of π … π stacking which also appear as a distinct pale green area at around $d_e = d_i = 1.8$ Å [70] in the FP.

ESP maps

The ESP is a measurable and fundamentally important physical property of compounds because it offers information on charge density distribution and molecular reactivity [61]. According to Fig. 9, positive ESP (red regions) is mostly dispersed on the parent skeleton, whereas negative ESP (blue areas) is concentrated on the borders of the molecules, particularly on the nitrogen and oxygen atoms of nitro groups, owing to their higher electronegativity. As can be seen from Fig. 9, the ESP of the intersection for

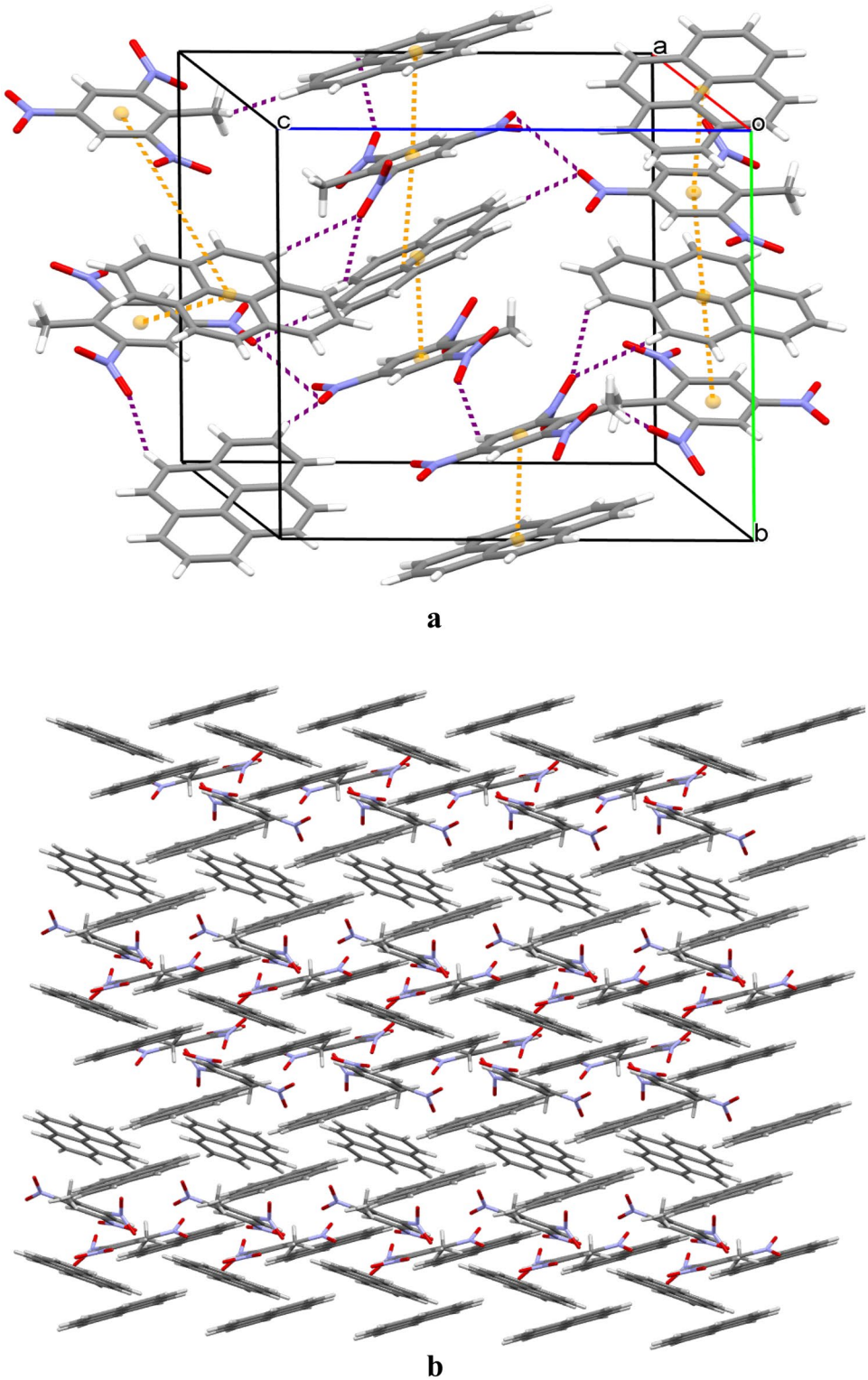


Fig. 3 **a** Crystal structure in unit cell of TNT:PYRN (purple dashed lines represent intermolecular hydrogen bonds; orange dashed lines indicate the π-stacking interactions between neighboring heterodimers). **b** Crystal packing of TNT:PYRN.

TNT:PYRN changes from red to light blue and a part of the red region changes to blue, indicating that the positive ESP between molecules decreases and a part of the positive ESP changes into negative ESP. All of the following alterations imply that variations in co-crystal charge distribution cause sensitivity changes.

NCI plots

The study of NCI and π-electron distribution structure provides crucial information in terms of the origin of molecular transformation, crystal packing, and stability [71, 72]. The

Table 4 Inter-molecular hydrogen bond lengths (Å)* and angles (°) of TNT:PYRN

D (donor)	H	A (acceptor)	D-H (Å)	H…A (Å)	D…A (Å)	D-H…A (°)
C (15)	H (15)	O (2)	0.95	2.59	3.426	146
C (21)	H (21)	O (2)	0.95	2.55	3.391	148
C (25)	H (25)	O (9)	0.95	2.49	3.413	163
C (26)	H (26)	O (10)	0.95	2.60	3.327	134

*Hydrogen bond (HB) lengths and angles are measured on Mercury 4.1.3 [51]

following relationship was projected by Chen et al. between the functions RDG and (*r*) [73].

$$\mathrm{RDG} = \frac{1}{2(3\pi^2)^{1/3}} \frac{|\nabla \rho(r)|}{\rho(r)^{4/3}} \tag{2}$$

$$(\Omega) = \mathrm{sign}\big(\lambda_2(r)\big)\rho(r) \tag{3}$$

where $\rho(r)$ is the electron density, and sign $(\lambda_2(r))$ is the sign of the second largest Hessian eigenvalue. The RDG maps contain multiple spikes. The spikes can be categorized into three groups: hydrogen bond region, vdW interaction region, and steric region, marked by blue, green, and red circles (Fig. 10d, e), respectively. More scatter dots in each region indicate higher electron density, implying a bigger contribution to overall interactions. Meanwhile, the strength of intermolecular interaction has a positive correlation with electron density in the corresponding region. The higher the electron density is, the stronger the intermolecular interaction is in each region. Then, turning to the vdW interaction region with ρ ranging from −0.02 to 0.005 a.u., it is seen that three possess stronger spikes and more points, indicating notable vdW interactions (Fig. 10b, d). From NCI plots of TNT:PYRN, it is clear that there are elliptical green slabs coloured light blue between TNT and the PYRN, which can be identified weak hydrogen bond interactions. As can be seen from Fig. 10b, c, and d, the electron density of TNT:PYRN in the steric region (ρ ranging from 0.01 to 0.02 a.u.) possesses stronger spikes indicating notable steric effect interactions. It can be concluded that TNT:PYRN provides the greatest reduction in steric effects, elevating its capability to disperse the impact energy to some extent. These co-crystal exhibit significant potential to develop energetic–non-energetic co-crystal as there are no strong intermolecular HBs in their molecules.

Detonation parameters for TNT:PYRN

Impact sensitivity

Table 6 shows the results of using a 10-kg drop weight in the BAM Fall Hammer equipment. The h_{50} values of TNT and TNT:PYRN were measured to be 25.1 cm (impact energy 25.1 J) and 70.8 cm (impact energy 70.8 J) respectively. The results also show that TNT:PYRN has a higher impact sensitivity than TNT, namely, safer explosive.

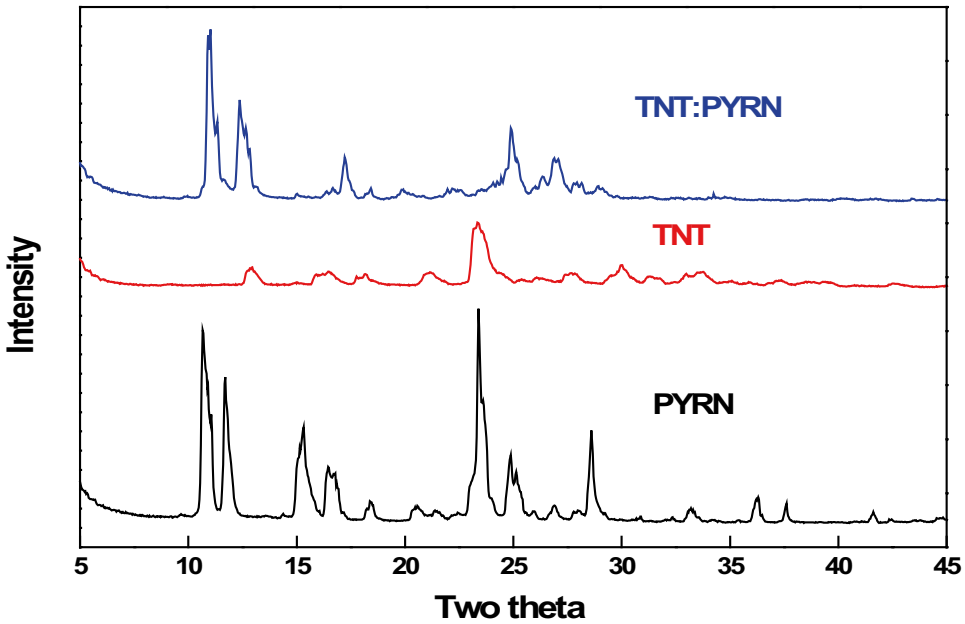


Fig. 4 Comparison of PXRD patterns for TNT, PYRN, and TNT:PYRN

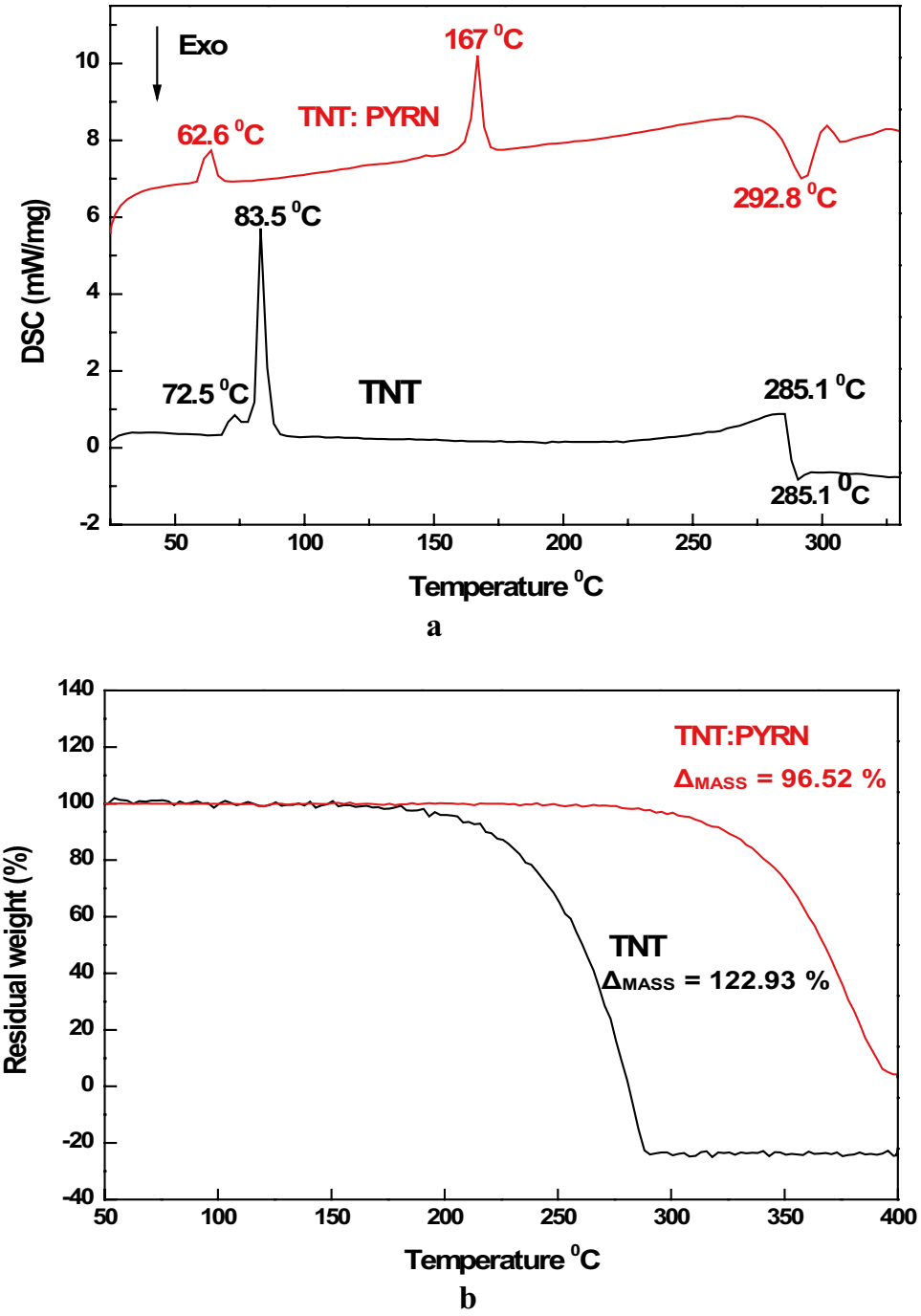


Fig. 5 **a** Differential scanning calorimetry plots. **b** Thermogravimetric analysis curves for TNT:PYRN.

Free space in the crystal lattice and packing coefficient

The free space, i.e., voids, and packing coefficient values of TNT and TNT:PYRN were calculated using Mercury CSD Ver. 4.1 [51]. The packing coefficient changed as a result of the formation of TNT:PYRN. Although TNT:PYRN is not denser than TNT, the synthesis of the novel compound significantly increased the packing coefficient and voids (Table 6). Additionally, higher compactness implies less free volume in the crystal, which promotes molecular degradation and the formation of hotspots, leading to greater insensitivity [74–76]. According to Table 6 and Fig. S1a-b, the calculated free space values are consistent with the impact sensitivity, indicating that it is less sensitive than TNT.

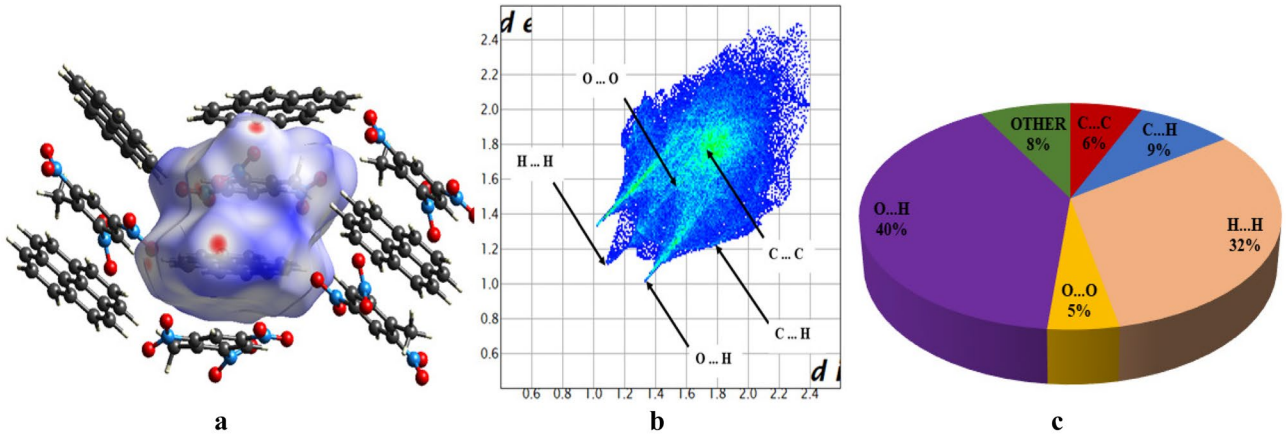


Fig. 6 **a** Hirshfeld surface mapped with d_{norm}. **b** 2D-fingerprint plots. **c** Populations of close intermolecular interatomic contacts of TNT:PYRN.

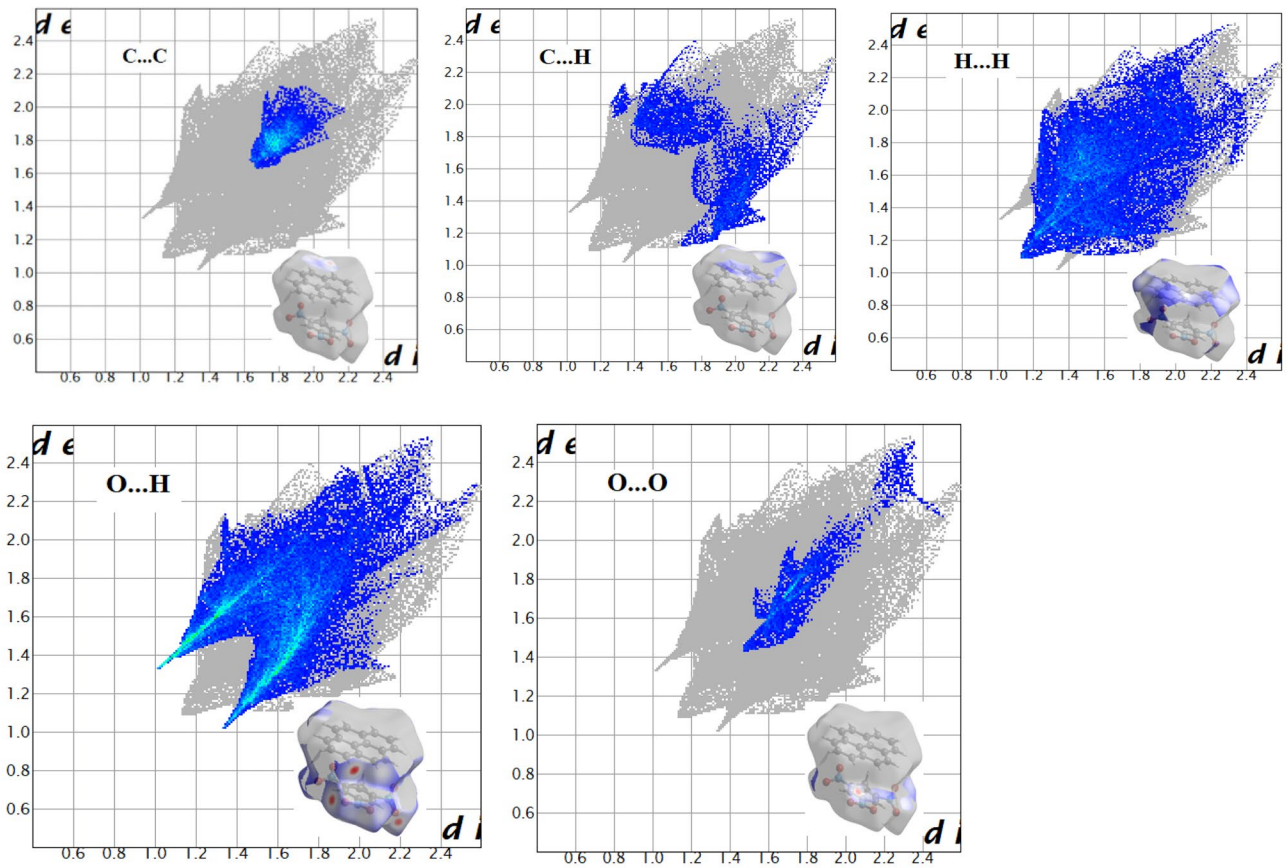


Fig. 7 Two-dimensional fingerprint plots for TNT:PYRN and showing contributions from different contacts

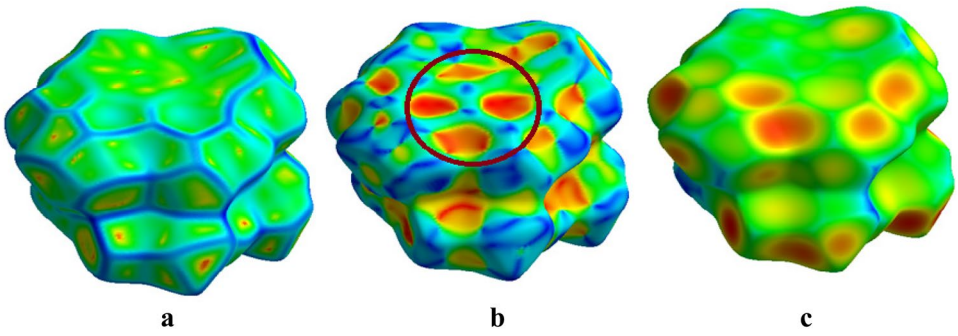


Fig. 8 TNT:PYRN is shown with the Hirshfeld surface mapped with **a** curvedness, **b** shape index, and **c** d_e

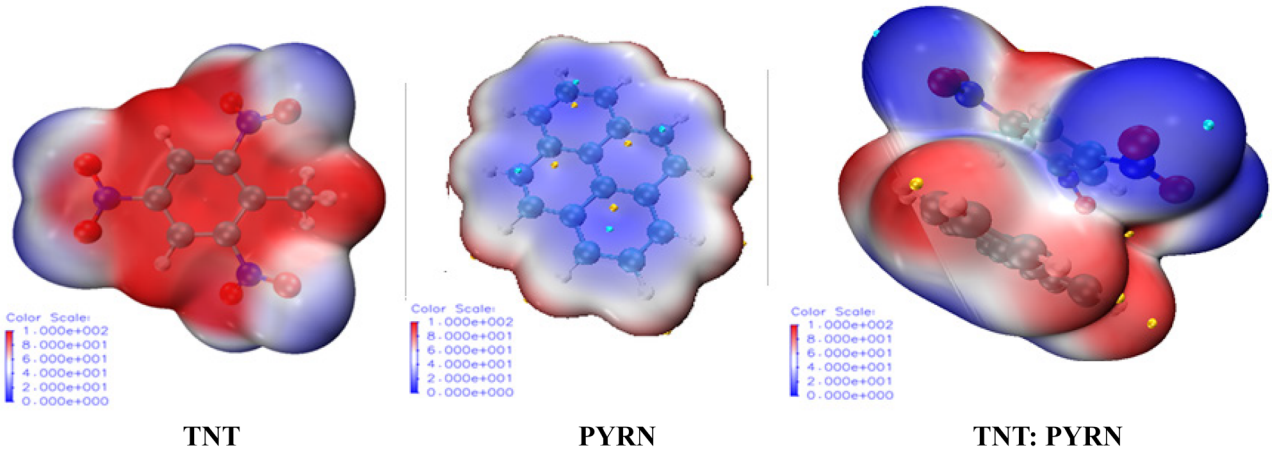


Fig. 9 Electrostatic potential surfaces representing charge density distributions of TNT, PYRN, and TNT:PYRN

Detonation performance

All explosion parameters were estimated with the software EXPLO5 V6.0. The software is based on the chemical equilibrium, steady-state model of detonation, and uses the Becker-Kistiakowsky-Wilson (BKW) equation of state for solid carbon [54]. The detonation parameters were computed at the CJ (Chapman-Jouguet condition) point, which is obtained from the Hugoniot curve of the system by its first derivative. For EXPLO5 calculations, the following set of BKW EOS parameters was used: $\alpha = 0.5$, $\beta = 0.38$, $\kappa = 9.32$, and $\theta = 4120$ [54]. The primary detonation products were thought to be C, H_2O, H_2, N_2, CH_4, C_2H_6, and CO_{26} (Fig. S2a-b.) Calculated standard heat of formation (ΔH_f°), oxygen balance (Ω), heat of detonation (Q), density (ρ), detonation velocity (D), and detonation pressure (P) values are indicated in and Fig. S2a-b and Table 6. The non-energetic co-former reduces detonation pressure and velocity as compared to pure TNT since it effectively dilutes the detonation reaction (Table 7).

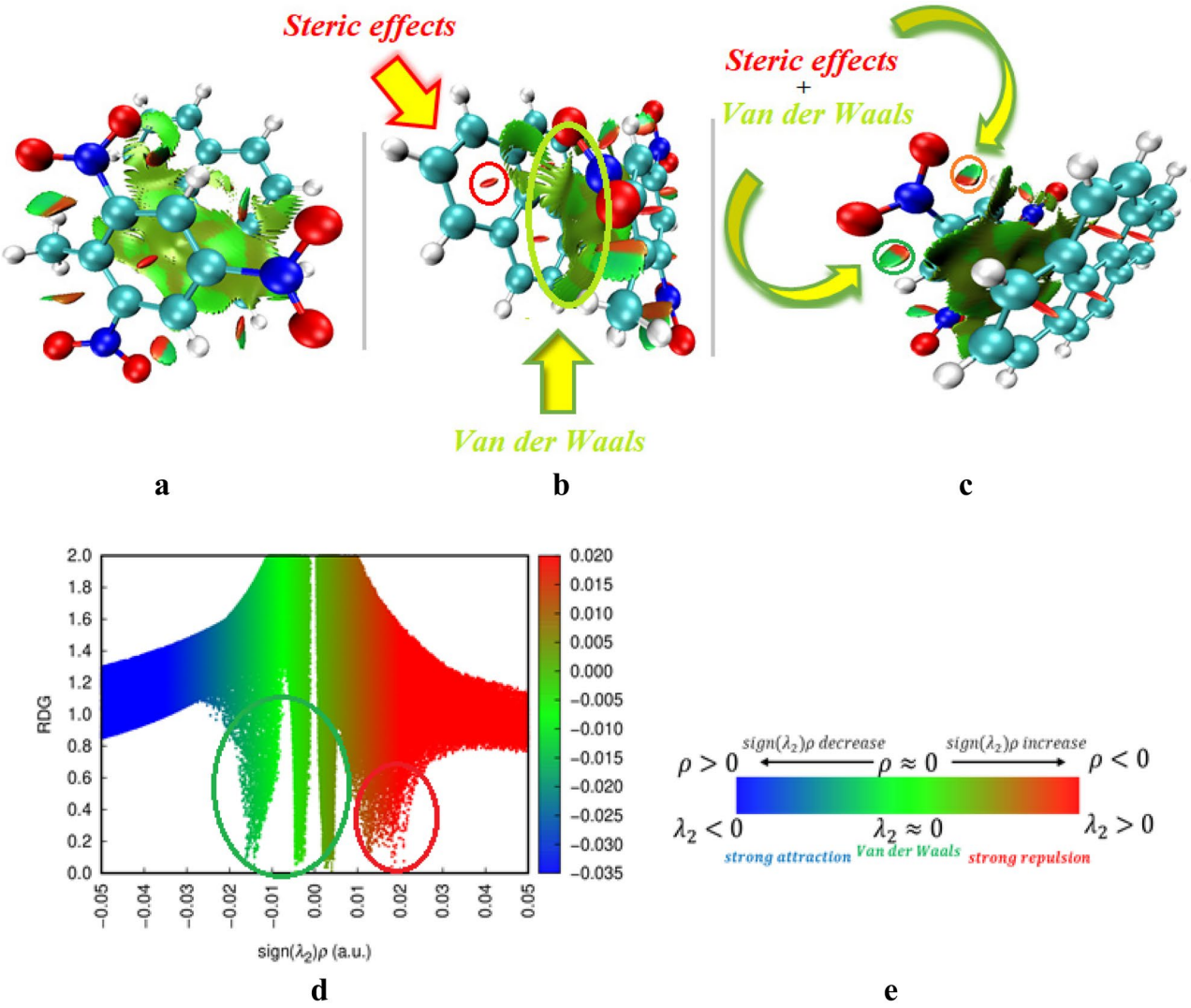


Fig. 10 RDG map and NCI plots of low-gradient isosurfaces ($s = 0.5$ a.u.) for TNT:PYRN co-crystal

Table 5 Melting points and the decomposition temperature of TNT, PYRN, and TNT:PYRN

Entry	Melting point (°C)	Decomposition temperature (°C)
TNT	83.5	285.1
PYRN	145–148	-
TNT:PYRN	167	292

Table 6 Comparison of the packing coefficient and free space of the unit cell of the TNT and TNT:PYRN

Entry	ρ (g·cm^{-3})	Packing coefficient (%)	Free space (voids)[a] (%)	Impact sensitivity (J)
TNT	1.68	72.1	13.1	25.1
TNT:PYRN	1.49	73.0	12.7	70.8

[a]Probe radius 0.2 Å, approx. grid spacing 0.5 Å

Table 7 Calculated detonation properties of TNT and TNT:PYRN

Component	Ω(%)[a]	ΔH_f° (kJ·mol^{-1})[b]	ρ (g·cm^{-3})[c]	D(km·s^{-1})[a]	P(GPa)[a]	IS(J)[d]
TNT	−73.98	25	1.68	7.00	20.02	25.1
TNT:PYRN	−176.9	33	1.49	5.29	8.48	70.8

[a]EXPLO5 V6.03

[b]CBS-4 M

[c]Calculated by using SCXRD data

[d]Impact sensitivity (BAM method)

Conclusion

A novel TNT:PYRN co-crystal explosive with a 1:1 molar ratio was synthesized by the co-crystallization method and characterized. Considering TNT has an electron poor system, it is proposed that compounds with electron-rich groups provide efficient formation opportunities with TNT in co-crystallization. The formation of co-crystal is mainly influenced by strong intermolecular π−π stacking interactions and weak hydrogen bond (C-H···O) interactions. Hirshfeld surfaces, NCI, and ESP analyses were used to find the noncovalent interaction and found the link between co-crystal structure and sensitivity. The obtained TNT:PYRN energetic co-crystal displayed a moderate value of heat of formation (−33.859 kJ·mol^{-1}), high melting point (T_m, 197 °C), high decomposition temperature (T_d, 293 °C), moderate detonation performance (Dv = 5.29 km·s^{-1}, P = 8.48 GPa), and excellent sensitivity towards outer stimuli, which suggest its potential as an insensitive explosive. The theoretical and experimental results have shown that TNT:PYRN not only highlight its potential application as a high-performance secondary explosive but also demonstrate the effectiveness of our new approach for designing and synthesizing high-performance insensitive EMs.

Supplementary Information The online version contains supplementary material available at https://doi.org/10.1007/s11224-023-02200-5.

Acknowledgements One of the authors (Nilgün Şen) would like to thank Professor Colin R. Pulham for his continual supervision and assistance during this study, as well as Dr. Gary Nichol for gathering single-crystal data sets at the University of Edinburgh's X-ray service department. Thanks are due again to the Cavendish Laboratory team at the University of Cambridge for granting access to the BAM Fall Hammer for impact sensitivity testing.

Author contribution All authors contributed to the study conception and design. Material preparation, data collection, and analysis were performed by Nilgün Şen and Nazife Aslan. The first draft of the manuscript was written by Nilgün Şen and all authors commented on previous versions of the manuscript. Methodology, formal analysis, and visualization were performed by Bayram Yüksel and Irem Teciman. All authors read and approved the final manuscript.

Funding This study was funded by the Scientific and Technological Research Council of Türkiye-TUBITAK-BIDEB 2219-International Postdoctoral Research Fellowship Program (Grant number: 1059B191600283).

Data availability The corresponding CIF files are available in the Cambridge Structural Database (CSD); for TNT: PYRN, the CCDC number is 1818100.

Code availability Not applicable.

Declarations

Competing interests The authors declare no competing interests.

Open Access This article is licensed under a Creative Commons Attribution 4.0 International License, which permits use, sharing, adaptation, distribution and reproduction in any medium or format, as long as you give appropriate credit to the original author(s) and the source, provide a link to the Creative Commons licence, and indicate if changes were made. The images or other third party material in this article are included in the article's Creative Commons licence, unless indicated otherwise in a credit line to the material. If material is not included in the article's Creative Commons licence and your intended use is not permitted by statutory regulation or exceeds the permitted use, you will need to obtain permission directly from the copyright holder. To view a copy of this licence, visit http://creativecommons.org/licenses/by/4.0/.

References

1. Dong H, Zhou F (1994) Properties of high energetic explosives and relatives. Science Press
2. Badgujar DM, Talawar MB, Asthana SN, Mahulikar PP (2008) Advances in science and technology of modern energetic materials: an overview. J Hazard Mater 151:289–305. https://doi.org/10.1016/j.jhazmat.2007.10.039
3. Zeman S (2003) In: Politzer P, Murray JS (ed) Energetic materials, Part 2. detonation, combustion. Elsevier: 25–52
4. Teipel U (2005) Energetic materials. Wiley-VCH, In particle processing and characterization
5. Pagoria PF, Lee GS, Mitchell AR, Schmidt RD (2002) A review of energetic materials synthesis. Thermochim Acta 384:187–204. https://doi.org/10.1016/S0040-6031(01)00805-X
6. Sabatini J, Oyler K (2016) Recent advances in the synthesis of high explosive materials. Crystals 6:5. https://doi.org/10.3390/cryst6010005
7. Chen J, Tang J, Xiong H, Yang H, Cheng G (2020) Combining triazole and furazan frameworks via methylene bridges for new insensitive energetic materials. Energetic Mater Front 1:34–39. https://doi.org/10.1016/j.enmf.2020.07.001
8. Zheng Y, Zhao X, Qi X, Wang K, Liu T (2020) Synthesis of 5-(1H-pyrazol-1-yl)-2H-tetrazole-derived energetic salts with

high thermal stability and low sensitivity. Energetic Mater Front 1:83–89. https://doi.org/10.1016/j.enmf.2020.08.004
9. Yao W, Xue Y, Qian L, Yang H, Cheng G (2021) Combination of 1,2,3-triazole and 1,2,4-triazole frameworks for new high-energy and low-sensitivity compounds. Energetic Mater Front 2:131–138. https://doi.org/10.1016/j.enmf.2021.05.002
10. Bu R, Jiao F, Liu G, Zhao J, Zhang C (2021) Categorizing and understanding energetic crystals. Cryst Growth Des 21:3–15. https://doi.org/10.1021/acs.cgd.0c01300
11. Zhang C (2018) On the energy & safety contradiction of energetic materials and the strategy for developing low-sensitive high-energetic materials. Chin J Energy Mater 26:2−10. https://doi.org/10.11943/j.issn.1006-9941.2018.01.001
12. Zhang C, Jiao F, Li H (2018) Crystal engineering for creating low sensitivity and highly energetic materials. Cryst Growth Des 18:5713–5726. https://doi.org/10.1021/acs.cgd.8b00929
13. Jiao F, Xiong Y, Li H, Zhang C (2018) Alleviating the energy &safety contradiction to construct new low sensitivity and highly energetic materials through crystal engineering. Cryst Eng Comm 20:1757−1768.https://doi.org/10.1039/C7CE01993A
14. Landenberger KB, Matzger AJ (2010) Cocrystal engineering of a prototype energetic material: supramolecular chemistry of 2,4,6-trinitrotoluene. Cryst Growth Des 10:5341–5347. https://doi.org/10.1021/cg101300n
15. Bolton O, Matzger AJ (2011) Improved stability and smart-material functionality realized in an energetic cocrystal. Angew. Chem. Int Ed 50:8960–8963. https://doi.org/10.1002/ange.201104164
16. Bolton O, Simke LR, Pagoria PF, Matzger AJ (2012) High power explosive with good sensitivity: a 2:1 cocrystal of CL-20:HMX. Cryst Growth Des 12:4311–4314. https://doi.org/10.1021/cg3010882
17. Zhang J, Shreeve JM (2016) Time for pairing: cocrystals as advanced energetic materials. Cryst Eng Comm 18:6124–6133. https://doi.org/10.1039/C6CE01239F
18. Liu G, Li H, Gou R, Zhang C (2018) Packing structures of CL-20-based cocrystals. Cryst Growth Des 18:7065–7078. https://doi.org/10.1021/acs.cgd.8b01228
19. Desiraju GR (1989) Crystal engineering: The design of organic solids. Elsevier
20. Desiraju GR (2013) Crystal engineering: from molecule to crystal. J.Am. Chem Soc 135:9952–9967. https://doi.org/10.1021/ja403264c
21. Saha S, Mishra MK, Desiraju GR (2018) From molecules to interactions to crystal engineering: Mechanical properties of organic solids. Acc Chem Res 51:2957–2967. https://doi.org/10.1021/acs.accounts.8b00425
22. MacGillivray LR (2017) Polymorphs, pseudopolymorphs and the crystal engineer: friends and foes. Acta Crystallogr A 73:C311
23. Sun C (2013) Cocrystallization for successful drug delivery. Expert Opin Drug Del 10:201–213. https://doi.org/10.1517/17425247.2013.747508
24. Sanphui P, Devi VK, Clara D, Malviya N, Ganguly S, Desiraju GR (2015) Cocrystals of hydrochlorothiazide: solubility and diffusion/permeability enhancements through drug-coformer interactions. Mol Pharmaceut 12:1615–1622. https://doi.org/10.1021/acs.molpharmaceut.5b00020
25. Du M, Li C, Liu C, Fang S (2013) Design and construction of coordination polymers with mixed-ligand synthetic strategy. Coordin Chem Rev 257:1282–1305. https://doi.org/10.1016/j.ccr.2012.10.002
26. Chen P, Li Q, Grindy S, Holten-Andersen N (2015) White-light-emitting lanthanide metalloges with tunable luminescence and reversible stimuli-responsive properties. J Am Chem Soc 137:11590–11593. https://doi.org/10.1021/jacs.5b07394
27. Wang S, McGuirk CM, D'Aquino A, Mason JA, Mirkin CA (2018) Metal-organic framework nanoparticles. Adv Mater 30:1800202. https://doi.org/10.1002/adma.201800202
28. Seetharaj R, Vandana PV, Arya P, Mathew S (2019) Dependence of solvents, pH, molar ratio and temperature in tuning metal organic framework architecture. Arab J Chem 12:295–315. https://doi.org/10.1016/j.arabjc.2016.01.003
29. Young JA (2008) Crystal engineering intermolecular hydrogen bond. Acta Crystallogr A 64:C640
30. Aakeroy CB, Epa K, Forbes S, Schultheiss N, Desper J (2013) Ranking relative hydrogen-bond strengths in hydroxybenzoic acids for crystal-engineering purposes. Chem Eur J 19:14998–15003. https://doi.org/10.1002/chem.201301402
31. Bulfield D, Engelage E, Mancheski L, Stoesser J, Huber SM (2020) Crystal engineering with multipoint halogen bonding: double two-point donors and acceptors at work. Chem Eur J 26:1567–1575. https://doi.org/10.1002/chem.201904322
32. Teyssandier J, Mali KS, De Feyter S (2020) Halogen bonding in two-dimensional crystal engineering. Chem Open 9:225−241.https://doi.org/10.1002/open.201900337
33. Ma Y, Zhang A, Zhang C, Jiang D, Zhu Y, Zhang C (2014) Crystal packing of low-sensitivity and high-energy explosives. Cryst Growth Des 14:4703–4713. https://doi.org/10.1021/cg501048v
34. Ma Y, Zhang A, Xue X, Jiang D, Zhu Y, Zhang C (2014) Crystal packing of impact-sensitive high-energy explosives. Cryst Growth Des 14:6101–6114. https://doi.org/10.1021/cg501267f
35. Zhang C, Wang X, Huang H (2008) π-stacked interactions in explosive crystals: Buffers against external mechanical stimuli. J Am Chen Soc 130:8359–8365. https://doi.org/10.1021/ja800712e
36. Tian B, Xiong Y, Chen L, Zhang C (2018) Relationship between the crystal packing and impact sensitivity of energetic materials. Cryst Eng Comm 20:837–848. https://doi.org/10.1039/C7CE01914A
37. Zhang J, Shreeve JM (2014) 3,3′-Dinitroamino-4,4′-azoxyfurazan and its derivatives: an assembly of diverse N-O building blocks for high-performance energetic materials. J Am Chem Soc 136:4437–4445.https://doi.org/10.1021/ja501176q
38. Zhang J, Parrish DA, Shreeve JM (2015) Curious cases of 3,6-dinitropyrazolo[4,3-c] pyrazole-based energetic cocrystals with high nitrogen content: an alternative to salt formation. Chem Commun 51:7337–7340. https://doi.org/10.1039/C5CC01745A
39. Şen N, Dursun H, Hope KS, Nazir H, Acar N, Atakol O (2020) Towards low-impact-sensitivity through crystal engineering: new energetic co-crystals formed between picric acid, trinitrotoluene and 9-vinylanthracene. J Mol Struct 1219. https://doi.org/10.1016/j.molstruc.2020.128614
40. Şen N (2019) Characterization and properties of a new energetic co-crystal composed of trinitrotoluene and 2,6-diaminotoluene. J Mol Struct 1179:453–461. https://doi.org/10.1016/j.molstruc.2018.11.013
41. Yang Z, Li H, Zhou X, Zhang C, Huang H, Li J, Nie F (2012) Characterization and properties of a novel energetic–energetic cocrystal explosive composed of HNIW and BTF. Cryst Growth Des 12:5155–5158. https://doi.org/10.1021/cg300955q
42. Wu JT, Zhang JG, Li T, Li ZM, Zhang TL (2015) A novel cocrystal explosive NTO/TZTN with good comprehensive properties. RSC Adv 5:28354–28359. https://doi.org/10.1039/c5ra01124h
43. Kurtay G, Şen N (2022) Improved stability of picric acid: 1-aminopyrene'charge-transfer complex: synthesis, characterization, energetic performance and molecular docking study. J Mol Struct 1262:133058. https://doi.org/10.1016/j.molstruc.2022.133058
44. Meyer R, Köhler J, Homburg A (2007) Explosives. John Wiley & Sons. Weinheim. 307−360
45. Ravi P, Badgujar DM, Gore GM, Tewari SP, Sikder AK (2011) Review on melt cast explosives. Propellants. Explos Pyrotech 36:393–403. https://doi.org/10.1002/prep.201100047
46. Klapötke TM (2022). Chemistry of High-Energy Materials. https://doi.org/10.1515/9783110536515

47. Ledgard JB (2007) The preparatory manual of explosives, 3rd edn. Lulu Publishing, Morrisville, Washington, USA
48. Sheldrick GM (2015) SHELXT – integrated space-group and crystal-structure determination. Acta Crystallogr Sect A Found Adv 71:3–8. https://doi.org/10.1107/S2053273314026370
49. Dolomanov OV, Bourhis LJ, Gildea RJ, Howard JAK, Puschmann H (2009) OLEX2: a complete structure solution, refinement and analysis program. J Appl Crystallogr 42:339–341. https://doi.org/10.1107/S0021889808042726
50. Sheldrick GM (2015) Crystal structure refinement with SHELXL. Acta Crystallogr Sect C Struct Chem 71:3–8. https://doi.org/10.1107/S2053229614024218
51. Mercury CSD 4.1.0 (Build 235316) (2022) https://www.ccdc.cam.ac.uk/mercury/
52. Kosanke KL, Sturman BT, Winokur RM and Kosanke BJ (2012) Encyclopedic dictionary of pyrotechnics, 1st edn. J Pyrotech, USA
53. Fuh CD, Lee JS, Liaw CM (2021) The design aspect of the bruceton test for pyrotechnics sensitivity analysis. J Data Sci 1:83–101. https://doi.org/10.6339/JDS.2003.01(1).119
54. Suceska M, Suceska M, EXPLO5, Version 6.01; Brodarski Institute, Zagreb, Croatia, EXPLO5 (2013). Version 6.01
55. McKinnon JJ, Spackman MA, Mitchell AS (2004) Novel tools for visualizing and exploring intermolecular interactions in molecular crystals. Acta Crystallogr B 60:627–668. https://doi.org/10.1107/S0108768104020300
56. Spackman MA, Turner MJ, McKinnon JJ, Wolff SK, Grimwood DJ, Spackman PR, Jayatilaka D (2017) Crystal Explorer 17. Univ. West. Aust. https://hirshfeldsurface.net
57. Frisch MJ, Trucks GW, Schlegel HB, Scuseria GE, Robb MA, Cheeseman JR, Scalmani G, Barone V, Petersson GA, Nakatsuji H, Li X, Caricato M, Marenich A, Bloino J, Janesko BG, Gomperts R, Mennucci B, Hratchian HP, Ortiz JV, Izmaylov AF, Sonnenberg JL, Williams-Young D, Ding F, Lipparini F, Egidi F, Goings J, Peng B, Petrone A, Henderson T, Ranasinghe D, Zakrzewski VG, Gao J, Rega N, Zheng G, Liang W, Hada M, Ehara M, Toyota K, Fukuda R, Hasegawa J, Ishida M, Nakajima T, Honda Y, Kitao O, Nakai H, Vreven T, Throssell K, Montgomery Jr. JA, Peralta JE, Ogliaro F, Bearpark M, Heyd JJ, Brothers E, Kudin KN, Staroverov VN, Keith T, Kobayashi R, Normand J, Raghavachari K, Rendell A, Burant JC, Iyengar SS, Tomasi J, Cossi M, Millam JM, Klene M, Adamo C, Cammi R, Ochterski JW, Martin RL, Morokuma K, Farkas O, Foresman JB, Fox DJ (2016) Gaussian 09, Rev. D.01, Gaussian Inc., Wallingford, CT
58. Dennington R, Keith T, Millam J (2009) GaussView, Version 5.0.8, GaussView, Version 5.0.8
59. Klapötke TM, Mieskes F, Stierstorfer J, Weyrauther M (2016) Studies on energetic salts based on (2,4,6-Trinitrophenyl) guanidine. Propellants. Explos Pyrotech 41:217–222. https://doi.org/10.1002/prep.201500338
60. Fischer D, Klapötke TM, Reymann M, Stierstorfer J (2014) Dense energetic nitraminofurazanes. Chem – A Eur J 20:6401–6411. https://doi.org/10.1002/chem.201400362
61. Johnson III RD (2015) NIST computational chemistry comparison and benchmark database (Release 17b): NIST Standard Reference Database Number 101
62. Jomaa I, Issaoui N, Roisnel T, Marouani H (2021) Insight into non-covalent interactions in a tetrachlorocadmate salt with promising NLO properties: experimental and computational analysis. J Mol Struct 1242:130730. https://doi.org/10.1016/j.molstruc.2021.130730
63. Tian L, Xu Y, Lin Q, Wang P, Lu M (2019) Syntheses of energetic cyclo -pentazolate salts. Chem – An Asian J. https://doi.org/10.1002/asia.201900776
64. Lu T, Chen F (2012) Multiwfn: a multifunctional wavefunction analyzer. J Comput Chem 33:580–592. https://doi.org/10.1002/jcc.22885
65. Humphrey W, Dalke A, Schulten K (1996) VMD: Visual molecular dynamics. J Mol Graph 14:33–38. https://doi.org/10.1016/0263-7855(96)00018-5
66. Loschen C, Klamt A (2012) Cosmo quick: a novel interface for fast σ-pro file composition and its application to cosmo-RS solvent screening using multiple reference solvents. Ind Eng Chem Res 51:14303–14308. https://doi.org/10.1021/ie3023675
67. Cruz Cabeza AJ (2012) Acid-base crystalline complexes and the pKa rule. Cryst Eng Comm 14:6362–6365. https://doi.org/10.1039/C2CE26055G
68. Molcanov K, Sabljica I, Kojic-Prodic B (2011) Face-to-face π-stacking in the multicomponent crystals of chloranilic acid, alkali hydrogenchloranilates, and water. Cryst Eng Comm 13:4211–4217. https://doi.org/10.1039/c1ce05161
69. Zhang H, Guo C, Wang X, Xu J, He X, Liu Y, Liu X, Huang H, Sun J (2013) Five energetic cocrystals of BTF by intermolecular hydrogen bond and π-stacking interactions. Cryst Growth Des 13:679–687. https://doi.org/10.1021/cg301353f
70. Bondi A (1964) Van der Waals volumes and radii. J Phys Chem 68:441–447. https://pubs.acs.org/doi/10.1021/j100785a001
71. Xie Z, Hu S, Cao X (2016) Theoretical insight into the influence of molecular ratio on the binding energy and mechanical property of HMX/2-picoline-N-oxide co-crystal, cooperativity effect and surface electrostatic potential. Mol Phys 114:2164–2176. https://doi.org/10.1080/00268976.2016.1190038
72. Lin H, Zhu S, Li H, Peng X (2013) Structure and detonation performance of a novel HMX/LLM-105 cocrystal explosive. J Phys Org Chem 26:898–907. https://doi.org/10.1002/poc.3188
73. Chen T, Zhang Y, Guo SF, Zhao LM, Chen W, Hao GZ, Xiao L, Ke X, Jiang W (2019) Preparation and property of CL-20/BAMO-THF energetic nanocomposites. Def Tech 15:306–312. https://doi.org/10.1016/J.DT.2018.08.013
74. Johnson ER, Keinan S, Mori-Sánchez P, Contreras-García J, Cohen AJ, Yang W (2010) Revealing non-covalent interactions. J Am Chem Soc 132:6498. https://doi.org/10.1021/JA100936W
75. Politzer P, Murray JS (2016) High performance, low sensitivity: conflicting or compatible? Propel Explos Pyrotech 41:414–425. https://doi.org/10.1002/prep.201500349
76. Xu Z, Yang H, Cheng G (2016) Studies on the synthesis and properties of polynitro compounds based on esteryl backbones. New J Chem 40:9936–9944. https://doi.org/10.1039/C6NJ02198K

Publisher's Note Springer Nature remains neutral with regard to jurisdictional claims in published maps and institutional affiliations.